(Received 5 March 2026, Accepted 13 April 2026, Scheduled 3 June 2026)

Analytical Modeling of Metamaterial Antennas and Their Equivalent Properties: A Characteristic Mode Approach

Mouad El Moudden[1], Badiaa Ait Ahmed[2, 3], and Otman Aghzout[1, *]

[1] *Department of AI and Digitalization, ISI Lab, ENSA-Tetouan, UAE, Tetouan, Morocco*
[2] *IACTEC Medical Technology Group, Instituto de Astrofísica de Canarias (IAC), San Cristóbal de La Laguna, Spain*
[3] *Universidad de La Laguna 38200, San Cristóbal de La Laguna, Santa Cruz de Tenerife, Spain*

ABSTRACT: This paper examines approaches to improving metamaterial antennas using the Theory of Characteristic Modes (TCM). We investigate the electromagnetic resonant modes of antenna elements, with a focus on how their material properties interact with their geometric configurations. The main goal is to enhance key features, such as bandwidth and radiation efficiency, in the electromagnetic modes of metamaterials. The study also examines how structural features, such as slots and metamaterial shapes, affect antenna performance. Split-ring resonators (SRRs) and complementary split-ring resonators (CSRRs) are considered to analyze how electric and magnetic modes can contribute to radiation efficiency using the approaches proposed in this paper. Important parameters, including characteristic angles, current distribution, bandwidth, and radiation patterns, are compared across different designs to identify the most efficient configurations. Notably, the analysis shows that when the SRR and CSRR structures are optimized, they can achieve similar radiation efficiency for electric and magnetic modes, respectively. Consequently, the TCM predictions are strongly corroborated by the S-parameter results. Overall, this paper provides practical insights into the design of compact and efficient metamaterial antennas and offers useful guidance for future wireless communication systems.

1. INTRODUCTION

Wireless communication systems are one of the most important parts of making sure that devices can talk to each other in a clear and efficient way. Wireless communication systems are important components of modern technology. They enable people to communicate for various purposes, including personal, industrial, and healthcare applications. The antenna is one of the most important parts of wireless communication systems because it enables devices to communicate with each other. Antennas are essential for enabling communication between devices, as they convert radio frequency (RF) signals passing through conductors into electromagnetic waves, thereby enabling communication between devices in different media. The literature contains a wide range of antenna designs for enabling communication in various applications [1, 2]. The essential parameters for evaluating antenna efficiency are return loss, bandwidth, and radiation patterns. A wide range of antennas is available for different purposes, including communication, radar, and navigation systems. The demand for compact devices is increasing, making microstrip antennas a popular choice for modern wireless communication systems, as this antenna is considered a simple, cost-effective, and easy-to-integrate component enabling communication between devices, meeting the need for compact devices [3]. However, many microstrip antennas are considered too large for wireless applications. Techniques that can be used to improve the performance of an antenna include the incorporation of slots into the patch [4], application of shorting posts, and utilization of substrates with high dielectric constants. Each of these techniques poses unique challenges that require further research. The performance of microstrip antennas is significantly related to the resolution of complex antenna design and placement problems [5].

Metamaterials possess unique approaches to resolving antenna problems. Some of the advantages offered by metamaterials include miniaturization, low weight, and affordability. Antenna performance can be enhanced through the use of SRRs and CSRRs, which allow for negative permeability and permittivity within particular frequency ranges. There are various reliable methods that can be employed in the evaluation of antenna performance, among them the employment of pseudo-random search and particle swarm optimization techniques [6]. Despite the extensive research that has been conducted, the properties of antennas need further investigation to address the challenges. With the growing need for enhanced performance in future wireless communication systems, the TCM has been established as a valuable method for optimizing antenna performance. First introduced by Garbacz and Turpin in the early 1970s [7] and later improved by Mautz and Harrington, the TCM has recently gained popularity because of its effectiveness in analyzing arbitrarily shaped antennas for various wireless applications [8, 9]. The usefulness of the TCM is based on its ability to offer a physical interpretation of the resonant frequency and radiation performance of an antenna design. The modes are solved numerically without excitation and are solely dependent on the dimensions and shape of the radiating structure. This ca-

* Corresponding author: Otman Aghzout (otmanaghzout@uae.ac.ma).

pability provides characteristic modes with a unique advantage over traditional methods employed in standard antenna design.

Several research works have shown that the characteristic modes are suitable for many types of antennas and microstrip with different shapes like circles, triangles, and rectangles. With the analysis of such structures, one can learn much about their behavior in electromagnetics and design optimized antennas. CMs can be calculated from the solution of the weighted eigenvalue equation:

$$XJ_n = \lambda_n R J_n \tag{1}$$

where X and R denote the imaginary and real components of the impedance matrix Z, respectively, in which $Z = R + jX$. The matrix $\mathbf{J}_n$ stands for the eigencurrent related to the n-th characteristic mode, while λ_n refers to the eigenvalue related to the same mode. A characteristic mode resonates when its eigenvalue $\lambda_n = 0$. The modal significance (MS) represents the contribution of each characteristic mode to radiation and is defined as:

$$MS_n = \frac{1}{\sqrt{1+\lambda_n^2}} \tag{2}$$

When ($MS_n = 1$), the characteristic mode is at resonance. Because radiated power depends on the modal significance, it follows that the bandwidth of the radiating mode can be estimated by the frequencies at which ($MS_n > 0.707$), which represents the half-power bandwidth. Characteristic Angle is another significant factor in the analysis of characteristic modes, and it is given as follows:

$$\alpha_n = 180^\circ - \tan^{-1}(\lambda_n) \tag{3}$$

The characteristic angle provides information about the nature of the mode. When ($\alpha_n = 180^\circ$), the mode is resonant. When ($\alpha_n < 180^\circ$), the mode is capacitive, and when ($\alpha_n > 180^\circ$), the mode is inductive. Therefore, the characteristic angle is an important parameter for determining the resonant behavior and radiation properties of the antenna.

Advanced wireless communication systems promise to revolutionize global connectivity by providing ultra-low latency, massive device connectivity, and high data transfer rates. Such systems promise to facilitate revolutionary applications, including self-driving cars, real-time virtual reality, and smart cities. To achieve this, however, there are a number of critical challenges that need to be addressed in the design of antennas, including optimizing the performance at higher frequencies, miniaturizing the design without compromising efficiency, and ensuring compatibility with new technologies. Such challenges must be addressed to advance the capabilities of new wireless systems.

The objective of this study is to contribute to the progress of research in this field by offering new solutions to the complexities of efficient antenna design. This study introduces a technique for an in-depth analytical investigation of metamaterial antennas by employing modern techniques of the TCM to enhance the performance characteristics of these antennas. This study aims to provide new insights into these antenna designs, which could result in efficient and flexible solutions in future communications. This study also examines the electromagnetic resonant modes of the components in a microstrip antenna, including their material and geometric configurations. The main goal is to optimize the performance characteristics of a metamaterial antenna using TCM. The study begins with the modeling of partial antenna elements to assess their behavior individually and in association with other antenna elements in the overall antenna structure. This detailed study could prove to be advantageous in gaining a better insight into the performance characteristics of the antenna. The role of TCM in identifying the resonant frequencies that can be used to enhance the efficiency of the antenna is also crucial. In addition, the study evaluates various structural configurations to understand the effect of the loaded elements, with the positions of the slots and metamaterials remaining constant. An analytical study is conducted without any excitation to find the resonances for the metamaterial antennas, particularly for the magnetic and electric mode configurations, to improve the efficiency of the antenna. This includes an exhaustive study of all the various parameters, such as characteristic angles, bandwidths, and currents. The primary contribution of this paper is the analysis of the characteristic modes of the electric and magnetic metamaterial structures CSRR and SRR together in a single circular microstrip antenna structure. This work differs from other works because the equivalence between electric and magnetic characteristic modes, including characteristic angles, modal significance, current distribution, and radiation pattern, is demonstrated for the first time. Additionally, the broad bandwidth effect in the proposed design is explained by using the characteristic mode overlapping theory, which provides the physics behind bandwidth enhancement due to modal interaction. Once the characteristic angles are derived for the antenna parameters, antenna designs are developed and validated for S-parameter analysis with guided waveport excitation. The analysis indicates a high level of consistency between TCM predictions and efficient S-parameter measurements to ensure high radiation efficiency. The conclusions of this paper offer innovative methods to enhance the design of metamaterial antennas for more efficient designs in future studies.

2. MODAL ANALYSIS OF ANTENNA ELEMENT INTERACTIONS

The TCM method can be employed to better understand the behavior of each element within a microstrip patch antenna. This approach involves analyzing the resonant modes of individual sections of the antenna and comparing them with the resonant frequencies of the complete antenna structure. By isolating and evaluating these modes, it is possible to determine the specific resonant frequencies at which each element contributes most actively to the overall radiation characteristics.

In this study, a simple microstrip patch antenna is considered with the following dimensions: 7.5 mm in length, 8.5 mm in width for the substrate with a thickness of 0.508 mm. The design process involved using a Rogers RT5880 material with a relative dielectric constant $\varepsilon_r = 2.2$. The designed microstrip patch antenna has a radiating circular patch with a radius of $R = 2.4$ and a thickness of $h = 0.035$ mm. The microstrip patch antenna and ground plane are assumed to be made of

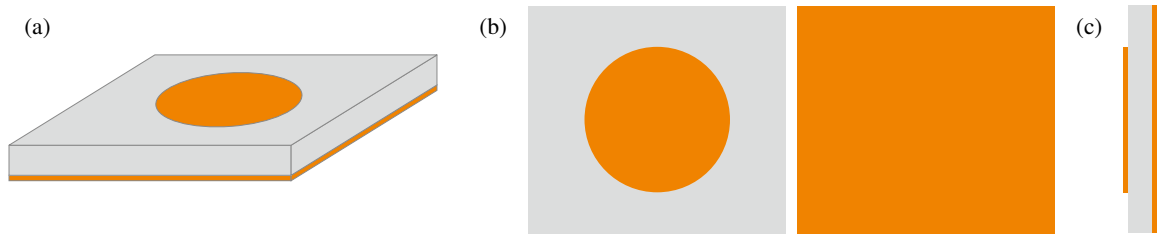

FIGURE 1. Geometry of the circular microstrip patch antenna, (a) Perspective View, (b) Top view, (c) Bottom view, (d) Side view.

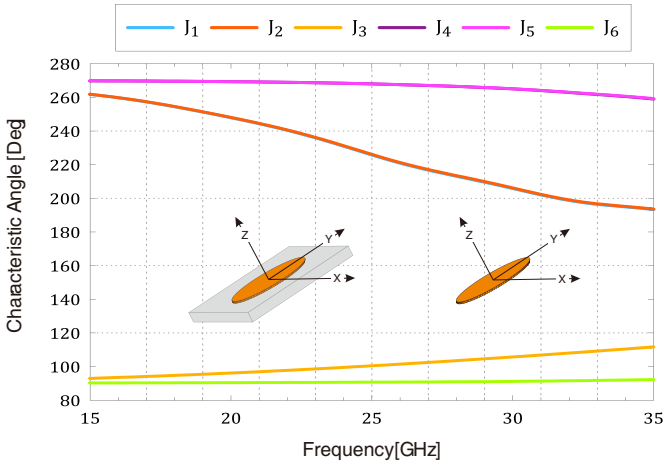

FIGURE 2. Variation with frequency of the characteristic angle for the resonant modes of the circular metallic patch on air and circular metallic patch on a Rogers RT5880 substrate.

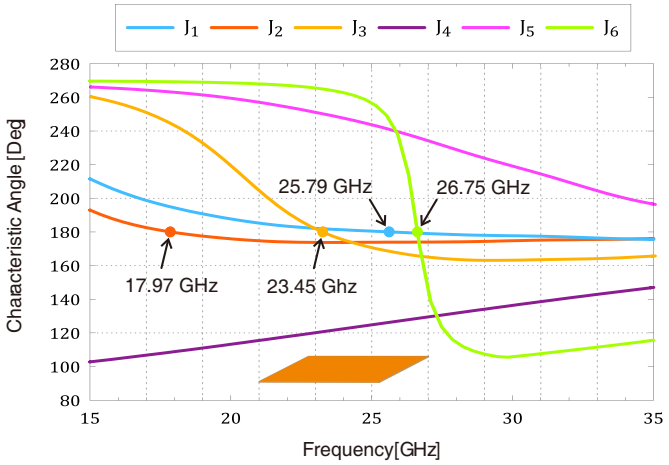

FIGURE 3. Variation with frequency of the characteristic angle for the resonant modes of the rectangular metallic plate in air.

perfect electric conductor (PEC) material. The geometry and configuration of the designed microstrip patch antenna are illustrated in Fig. 1. The analysis of the designed patch was conducted in a free space environment. In this environment, the patch was subjected to a plane wave. This analysis was performed to understand the basic electromagnetic properties of the designed patch. To enable a better and more comprehensive analysis of the properties of the designed patch, the analysis of its distinct modes was conducted.

Building on this preliminary investigation, a Rogers RT5880 substrate is presented, similar to the circular metallic patch that has already been analyzed. The substrate, with a relative dielectric constant $\varepsilon_r = 2.2$ and loss tangent of 0.0009, is useful for analyzing the impact of the substrate on the patch and the performance of the patch as an antenna. Characteristic angle is an important parameter that is considered while performing the modal analysis of the circular patch, with the objective of identifying the modes that facilitate the process of radiation. The characteristic angle is a critical parameter used in the modal analysis of the circular patch to understand the modes involved in radiation. This parameter provides structural insights into the resonant properties of the patch and the transition of stored energy between magnetic and electric fields within the structure. Modes operating in capacitive regions resonate when the characteristic angle is 180°, while modes in inductive regions appear beyond their resonance.

By evaluating the characteristic angle (CA), the behavior of the circular patch across various operating bands can be thoroughly understood, thereby enabling the design and optimization of efficient radiators. The identification of the first six modes for both the circular metallic patch in free space and on a Rogers RT5880 substrate can be achieved by analyzing the CA curve shown in Fig. 2. The analysis shows that all these modes correspond to non-resonant electric modes, which further proves that the patch is storing and switching energy rather than efficiently radiating energy at these modes. Moreover, the introduction of the Rogers RT5880 substrate does not have a major impact on the resonant behavior of the circular patch. This analysis further proves the minimal impact of the substrate on the circular patch and its ability to maintain its performance despite the introduction of the substrate material. The geometry of the structure under consideration is a rectangular metallic plate, chosen to analyze the behavior of the characteristic modes in a planar conducting structure in free space. This metallic plate was chosen to be the ground plane in the subsequent antenna analysis. It is assumed to be made of PEC material with the following dimensions: length $L_s = 8.5$ mm, width $W_s = 7.5$ mm, and thickness $h = 0.035$ mm. Fig. 3 shows the variation of the CA with frequency for the first six modes of the rectangular metallic plate in free space.

The resonance frequencies of the modes for the rectangular metallic plate in air can be directly determined from the characteristic angle versus frequency plot for the first six modes, as

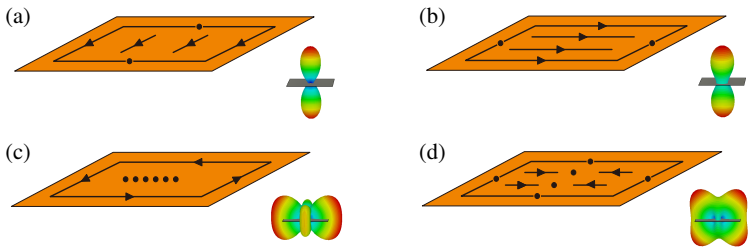

FIGURE 4. Characteristic current distributions and radiation patterns corresponding to the rectangular metallic plate on air, (a) mode J_1 at 25.79 GHz, (b) mode J_2 at 17.97 GHz, (c) mode J_3 at 23.45 GHz, (d) mode J_6 at 26.75 GHz.

depicted in Fig. 3. The analysis reveals that modes J_1 resonate at 25.79 GHz, mode J_2 at 17.97 GHz, mode J_3 at 23.45 GHz, and mode J_6 at 26.75 GHz, respectively. In contrast, modes J_4 and J_5 are non-resonant because their characteristic angles do not pass through $180°$. The radiating bandwidth of each mode can also be derived from the characteristic angle curves. The lower and upper boundaries of the radiating band correspond to $f_L = 135°$, and the upper boundary to $f_H = 225°$. According to the results in Fig. 3, modes J_1 and J_2 exhibit the narrowest radiating bandwidths. Mode J_3 remains close to $180°$ but does not cross $135°$, resulting in an effectively infinite bandwidth. Among the analyzed modes, only J_6 demonstrates a finite bandwidth of 5.64%. The reason for such a large bandwidth of the considered antenna is associated with the modal overlapping phenomenon in the context of characteristic mode theory. Namely, since many resonant modes are located very close to one another in frequency, their significance overlaps with each other. As a consequence, this phenomenon provides a continuous radiation region across the whole frequency band where the modes overlap, leading to an extremely wide bandwidth even above 100%.

Characteristic current distributions and their corresponding radiation patterns for the rectangular metallic plate on air at their respective resonance frequencies are illustrated in Fig. 4. Modes J_1 and J_2 exhibit a single predominant current direction, characterized by vertical and horizontal currents, respectively. This organized current flow results in radiation patterns that produce bidirectional beams. Mode J_1 achieves a maximum directivity of 5.79 dBi, whereas mode J_2 achieves a higher directivity of 3.86 dBi. In contrast, mode J_3 is characterized by a combination of vertical and horizontal currents, whereas mode J_6 features two variations in the current direction. These complex current distributions give rise to radiation patterns with multiple beams, with the number and orientation of beams determined by the mode order. The directivity achieved by mode J_3 is slightly higher with a value of 3.2 dBi, whereas the minimum directivity achieved by mode J_6 is 2.1 dBi. The radiation behavior of any characteristic mode is determined by its current distribution and effective radiating aperture. Those modes with uniform current distributions directed along some preferred direction possess high radiation intensities in this direction, and therefore have high directivity. Modes with complex and multidirectional current distributions result in radiation beams distributed in different directions, leading to poor directivity. This explanation clarifies the physical sense of the results obtained.

A detailed examination and analysis of the different components of the microstrip patch antenna will provide a better understanding of the characteristic modes of the integrated circular microstrip patch antenna. This analysis will focus on the different contributions of each component to the characteristic modes of the antenna. An analysis of the different changes in the design, structure, and configuration of the different components of the microstrip patch antenna will provide an idea of the effect of these components on the characteristic modes, which would, in turn, affect the performance of the circular microstrip patch antenna. Fig. 5 shows the variation of the characteristic angle with frequency for the first six modes of the circular microstrip patch antenna. The non-resonant nature of the capacitive modes J_1 and J_6 is evident because the angles associated with these modes are greater than $180°$. Mode J_2 resonates at 32.10 GHz, mode J_3 resonates at 20.44 GHz, mode J_4 resonates at 34.91 GHz, and the inductive nature of mode J_5 is evident. From the characteristic angle plots, it is evident that the bandwidths over which the antenna's modes radiate are extremely wide, qualifying them as broadband radiators with bandwidths exceeding 100%.

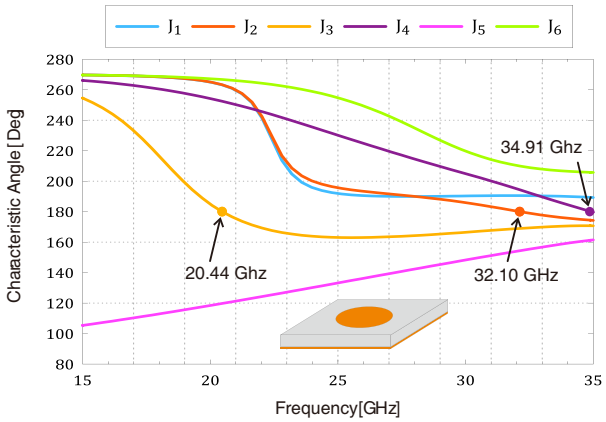

FIGURE 5. Characteristic angle associated with the first six modes of the circular microstrip patch antenna.

Figure 6 illustrates the characteristic current distributions and radiation patterns for the circular microstrip patch antenna. Mode J_2 exhibits a unidirectional current flow, primarily characterized by horizontal currents. This mode produced a broadside radiation pattern with the maximum field oriented in the z direction. In contrast, mode J_3 displayed a combination of vertical and horizontal currents, whereas mode J_4 revealed two

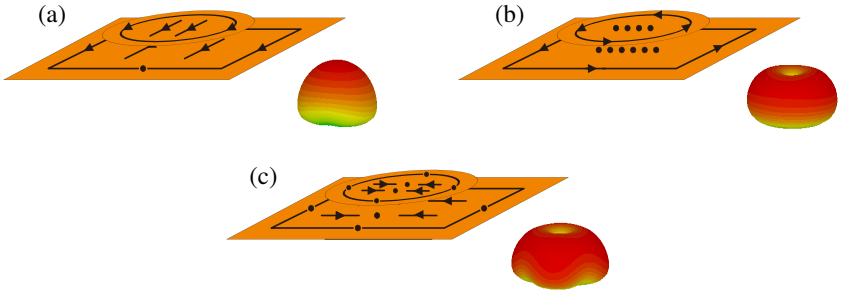

FIGURE 6. Characteristic current distributions and radiation patterns corresponding to the circular microstrip patch antenna, (a) mode J_2 at 32.1 GHz, (b) mode J_3 at 20.44 GHz, (c) mode J_4 at 34.91 GHz.

distinct variations in current direction. Both J_3 and J_4 generated radiation patterns with a null at the central line, indicating suppressed radiation in the z direction. The directivities of the three resonant modes were found to be 8.66 dBi, 6.17 dBi, and 5.64 dBi, respectively. From the above results, it was observed that the radiation characteristics and directivity varied for different current distributions. The analysis of the circular microstrip patch antenna and its individual components using TCM provided crucial insights into the resonant characteristics of the microstrip patch antenna. From the characteristic angle plots, it was observed that the circular patch antenna in free space and on a Rogers RT5880 substrate exhibited non-resonant electric modes. The addition of the substrate does not alter the resonant characteristics of the patch antenna. This is evidence of the stability of the circular patch antenna in maintaining its characteristics even when mounted on a substrate. The TCM of the rectangular metallic plate in air was found to exhibit distinct resonant modes at frequencies of 17.97 GHz, 23.45 GHz, 25.79 GHz, and 26.75 GHz. Modes J_1 and J_2 exhibited the highest directivity owing to their uniform current distributions along the axes. Modes J_3 and J_6 exhibited complex current distributions, thereby showing multiple beam radiation patterns. The integrated circular patch antenna displayed a mix of resonant and non-resonant modes. Mode J_2 had a resonant frequency of 32.1 GHz and a maximum directivity of 8.66 dBi. This indicates a strong broadside radiation pattern. Modes J_3 and J_4 produced multi-beam radiation patterns as a result of the complex current distributions. These two modes had a slightly lower directivity. The wide radiating bandwidths obtained from the characteristic angle plots show promise for broadband operation. This is an advantage for applications where a wide coverage is required. The study proved that TCM is an effective method for the performance analysis of microstrip patch antennas. From the analysis of the individual components and the combination, it can be concluded that the resonant characteristics of the circular microstrip patch antenna remain the same. This is an indication of the suitability of this patch for robust antenna designs. The rectangular ground plane contributed specific resonant modes for improving the radiation characteristics. The combination of all the components produced a broadband antenna with a high directivity level and well-defined radiation patterns.

3. MODAL ANALYSIS OF METAMATERIAL STRUCTURES

3.1. Fundamental Concepts and Physical Properties of Metamaterial Structures

Metamaterials are a particular class of materials that are used to design a specific category of materials that have unique properties that are not available in nature. It has to be noted that metamaterials are very different from other materials in the sense that the unique properties that are exhibited are not a result of the constituent parts' chemistry, but it is more related to the way in which the geometry is arranged [10]. It has to be noted that the size of the unit cells in the metamaterial is much smaller than the wavelength of the electromagnetic waves that are used. Due to this fact, it can be stated that the metamaterial can be considered to be homogeneous in nature when the waves are used. Due to the unique properties that can be achieved in the design of the unit cells, it can be stated that metamaterials can be used to achieve properties that are not possible in any other materials [11]. It has to be noted that the unique properties that can be achieved in metamaterials are a result of the manipulation that is achieved in the constitutive parameters such as permeability (μ) and permittivity (ε). On the other hand, permittivity controls the way the material behaves when it is exposed to an electric field, while permeability controls the way the material behaves when it is exposed to a magnetic field. By using these parameters, engineers have the ability to create materials that have unique characteristics, like negative refraction, which cannot be found naturally. The ability to control the permittivity and permeability of the metamaterial creates the opportunity to create sophisticated electromagnetic devices, which could be used to create communication systems and imaging technology.

The classification of metamaterials can be based on the signs of their permittivity (ε) and permeability (μ). This classification results in four major types of metamaterials. The first type is double-positive (DPS), in which the permittivity (ε) and permeability (μ) are positive [12]. Such types of materials are similar to normal dielectrics and are known as right-handed (RH). Materials in this category follow the normal right-hand rule, in which the wave propagation direction, electric field, and magnetic fields are related in a specific manner [13]. This class of material includes natural materials, such as glass and air. Epsilon negative (ENG) materials are characterized by nega-

tive permittivity ($\varepsilon < 0$), while their permeability is positive ($\mu > 0$). This class of material displays unusual properties such as wave inhibition in certain frequency bands and can be fabricated using parallel plate capacitors and wire arrays that are capable of interacting with the electric component of electromagnetic waves [14]. The third class of material is mu negative (MNG), whose characteristics are negative permeability ($\mu < 0$), while its permittivity is positive ($\varepsilon > 0$). MNG materials are less common than their ENG counterparts and can be synthesized using specific resonant structures, such as split-ring resonators that can interact with the magnetic field component of electromagnetic waves and exhibit unusual properties [15]. Finally, the class of double negative (DNG) materials has negative values of permittivity and permeability ($\varepsilon < 0$, $\mu < 0$) [16]. DNG materials are also known as left-handed materials as they violate the right-hand rule, causing the wave vector to reverse its direction in comparison to the electric and magnetic fields [17]. DNG materials can sustain backward wave propagation, showing negative refraction properties [18]. The engineering of DNG materials has the potential to revolutionize the design of optical and microwave devices such as metamaterial lenses and antennas [19].

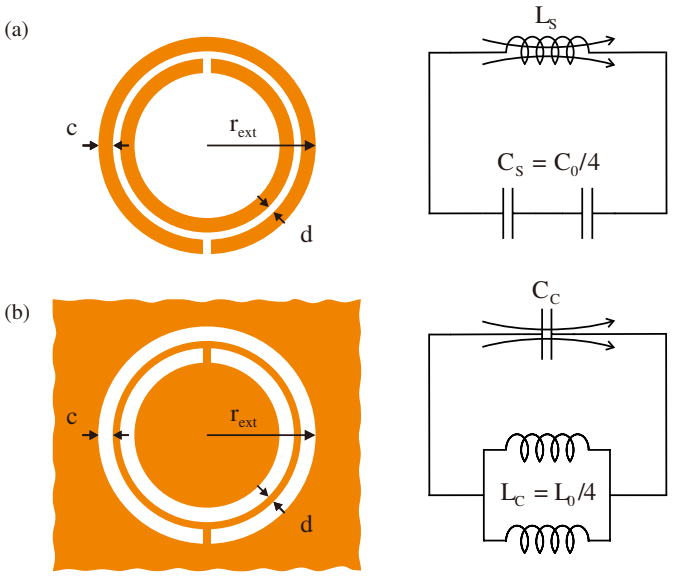

FIGURE 7. Topologies and their equivalent-circuit models of the (a) SRR, (b) CSRR.

In this work, the role of SRRs and CSRRs is investigated for the contribution they make towards the design of metamaterials [20], as shown in Fig. 7. The structures were analyzed for the case in which they were integrated with a microstrip patch antenna on a Rogers RT5880 substrate, with a relative permittivity of $\varepsilon_r = 2.2$. The structure of the SRRs, as illustrated in Fig. 8(a), consists of concentric metallic rings with gaps inserted between them strategically. When an external electromagnetic field is applied, the concentric rings produce resonating magnetic fields, resulting in the flow of currents that generate a magnetic field [21]. This phenomenon is a basic requirement for the creation of negative permeability, which is an essential requirement for the creation of left-handed materials [22]. In contrast, CSRRs can be achieved by etching complementary split-ring structures on a conductive surface, in place of using actual metallic rings [23]. These structures primarily respond to the electric-field component of electromagnetic waves, which enables the achievement of negative permittivity [24]. This research considers both SRRs and CSRRs, aiming to clarify the roles of these structures in the manifestation of special properties, thus contributing to the improvement of antennas and other devices that require adaptive changes in the electromagnetic properties of the materials they contain. For the SRR antenna, the electric field is mainly concentrated around the areas of the concentric rings, which have gaps, as a result of the disruption of the flow of the electric current, thereby causing a strong electric field to be radiated outward but remaining localized around the areas of the gaps, as shown in Fig. 8(b). The magnetic field distribution has the form of loops around the concentric rings, as a result of the induced currents from an external source of excitation. The areas of the gaps, which result from the disruption of the flow of the electric current, form a quasi-static magnetic field, as shown in Fig. 8(c).

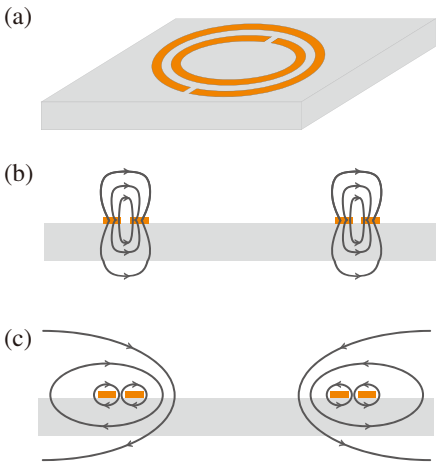

FIGURE 8. Behavior of the field lines for the SRR antenna: (a) geometry, (b) electric field lines, (c) magnetic field lines.

For the CSRR antenna, the electric field is primarily concentrated within the slots, where the field lines connect both ends of the slots as illustrated in Fig. 9(a). The intensity of the

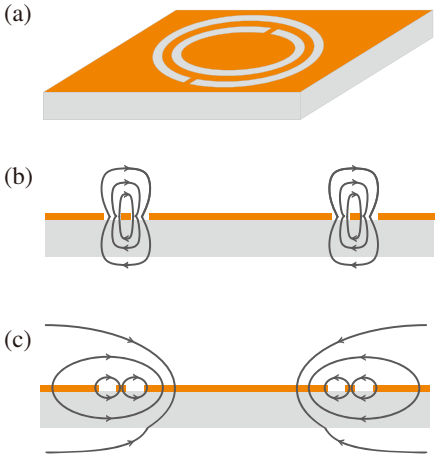

FIGURE 9. Behavior of the field lines for the CSRR antenna: (a) geometry, (b) electric field lines, (c) magnetic field lines.

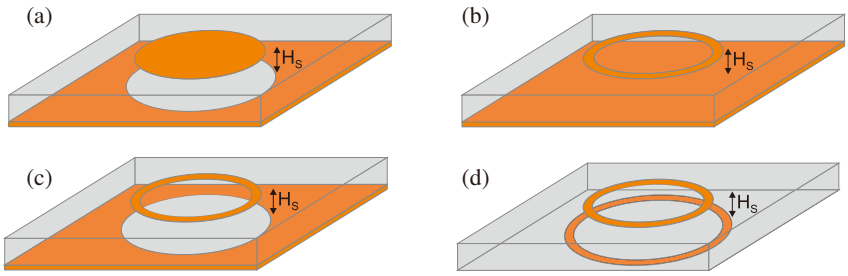

FIGURE 10. The geometry of the circular microstrip patch antenna with slots at different positions, (a) circular microstrip patch antenna with circular slot in ground plane, (b) circular microstrip patch antenna with circular slot in patch, (c) microstrip ring resonator antenna with circular slot in ground plane, (d) microstrip double-ring resonator antenna.

electric field is also concentrated at the edges of the slots, particularly at the gaps. This emphasizes the importance of the substrate for the electric field. The electric field is intricately related to the geometry of the slots. The electric field lines for the CSRR antenna are shown in Fig. 9(b). The magnetic field for the CSRR antenna is a result of the current flowing along the edges of the slots in the form of loops in a plane parallel to the slots. The intensity of the magnetic field is the highest at the positions of the slots, where the current density is also highest. The presence of gaps within the slots also affects the intensity of the magnetic field. The presence of these gaps results in a higher intensity of the closed-loop pattern within the near-field region. Fig. 9(c) shows the magnetic field lines for the CSRR ntenna. The distinctions between SRR and CSRR can be made on the basis of their relation to the electromagnetic field. The SRR structure is mainly dependent on the magnetic component of the electromagnetic wave, creating a negative permeability property, while the CSRR is more concerned with the electric field component that gives rise to a negative permittivity property. When considering the characteristic modes, it can be said that SRR introduces magnetic resonant modes while CSRR produces electric resonant modes. In spite of the differences in the properties produced by SRR and CSRR, both types of antennas create comparable radiation properties, since they produce comparable resonant modes.

These SRRs and CSRR antenna configurations have proven particularly advantageous in situations where a wider radiation pattern is required or where electromagnetic confinement is minimized. Their field distributions and resonance characteristics have made them particularly suitable for use in advanced antenna structures.

3.2. Design and Performance Analysis of Circular Microstrip Patch Antennas with Integrated Metamaterial Slots

The increasing need for high-performance antennas has led to the development of new techniques in the field of antenna design and the materials used to construct antennas. Among the new techniques used to improve antenna performance is the use of metamaterials to improve the functionality of antennas.

The objective of this study was to design metamaterial antennas by inserting slots at different locations on the microstrip patch antenna, with the intention of improving the antenna performance using the capabilities of metamaterials and slots to improve the functionality of the microstrip patch antenna. The geometric configuration of the circular microstrip patch antenna with slots at various locations is depicted in Fig. 10. These circular slots were cut from the ground plane and the patch antenna. This antenna design aimed to study the effects of slots on several antenna parameters and radiation characteristics. Fig. 11 shows the change in the characteristic angle with frequency for the first six modes of the circular microstrip patch antenna with slots at various locations.

As shown in Fig. 11(a), the circular microstrip patch antenna with a circular slot in the ground plane, having a radius of 2.6 mm, exhibits three degenerated resonant modes. Mode J_1 resonates at 32.06 GHz, mode J_3 at 29.29 GHz, and mode J_4 at 19.70 GHz. Mode J_5 is non-resonant with inductive energy, whereas modes J_2 and J_6 are non-resonant with capacitive energy. In Fig. 11(b), the circular microstrip patch antenna with a circular slot in the patch, having a radius of 2 mm, exhibits four degenerated resonant modes. Mode J_1 resonates at 19.95 GHz, mode J_2 at 31.61 GHz, mode J_3 at 20.43 GHz, and mode J_4 at 32.26 GHz. However, modes J_5 and J_6 are non-resonant and store inductive and capacitive energy, respectively. Fig. 11(c) shows the microstrip ring resonator antenna with a circular slot in the ground plane, which exhibits four degenerated resonant modes. Mode J_1 resonates at 28.86 GHz, mode J_2 at 21.11 GHz, mode J_3 at 19.98 GHz, and mode J_4 at 19.75 GHz. Modes J_5 and J_6 are non-resonant and store capacitive and inductive energy, respectively. Finally, in Fig. 11(d), the microstrip double-ring resonator antenna exhibits four degenerated resonant modes. Mode J_1 resonates at 21.75 GHz, mode J_2 at 29.06 GHz, mode J_3 at 21.65 GHz, and mode J_4 at 29.10 GHz. Modes J_5 and J_6 are non-resonant and store inductive energy.

Additionally, the radiating bandwidth of the modes can be determined using the information provided by the plots of the characteristic angle, as shown in Fig. 11. In particular, in Fig. 11(a), modes J_1 and J_4 are broadband radiators with an associated radiating bandwidth larger than 100%, because the CA remains close to 180°, and it does not pass through 135°. Only mode J_3 has a bandwidth of 22.87%. In Fig. 11(b), the modes J_1, J_2 and J_3 are broad band radiators with an associated radiating bandwidth larger than 100%, except for mode J_4 which has a bandwidth of 21.92% after adding a slot to the patch. In Fig. 11(c), the modes J_1, J_2, and J_3 have bandwidths of

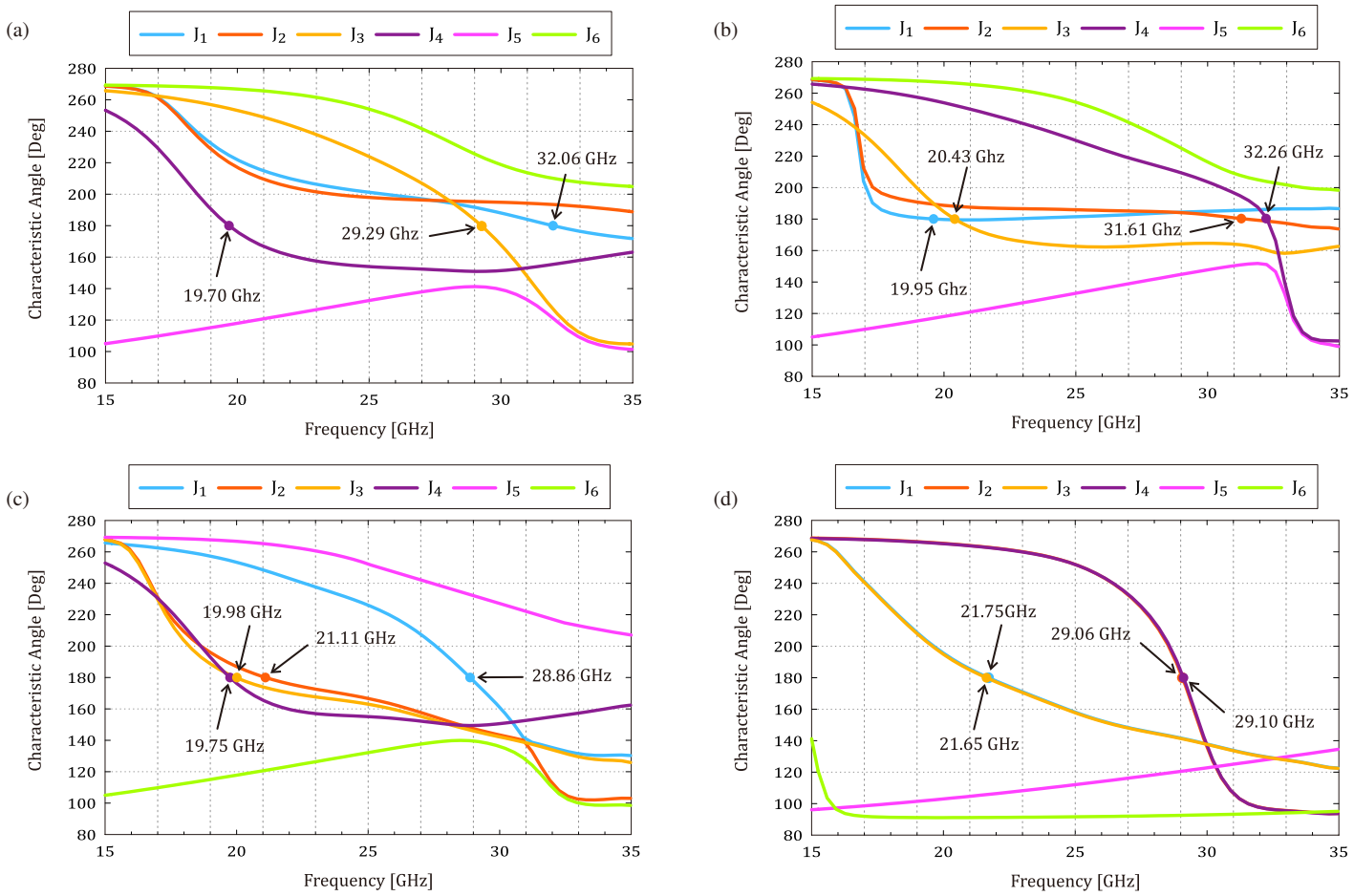

FIGURE 11. The variation with frequency of the characteristic angle for the first six modes of (a) circular microstrip patch antenna with circular slot in ground plane, (b) circular microstrip patch antenna with circular slot in patch, (c) microstrip ring resonator antenna with circular slot in ground plane, (d) microstrip double-ring resonator antenna.

23.81%, 65.86%, and 73.13%, respectively, after adding a slot to the ground plane. Conversely, mode J_4 is a broad band radiator with an associated radiating bandwidth larger than 100%. For the last structure shown in Fig. 11(d), the modes J_1, J_2, J_3 and J_4 have bandwidths of 58.64%, 8.67%, 59.04% and 8.57%, respectively.

The characteristic current distributions and radiation patterns corresponding to the circular microstrip patch antenna with a circular slot in the ground plane at each of its resonance frequencies are shown in Fig. 12. It can be observed that mode J_1 exhibits a concentrated current flow around both the ground plane and the slot, with horizontal currents on the patch, highlighting a strong coupling between these sections. Mode J_1 generates a bi-directional radiation pattern with the maximum field strength in the $\pm z$ direction. In contrast, mode J_3 displays two distinct variations in current direction, whereas mode J_4 shows a combination of vertical and horizontal currents. Both modes J_3 and J_4 produce bi-directional radiation patterns exhibiting a null at the focal point, indicating suppressed radiation in the $\pm z$ direction. The measured directivities of the three resonant modes were 4.45 dBi, 4.47 dBi, and 4.10 dBi, respectively.

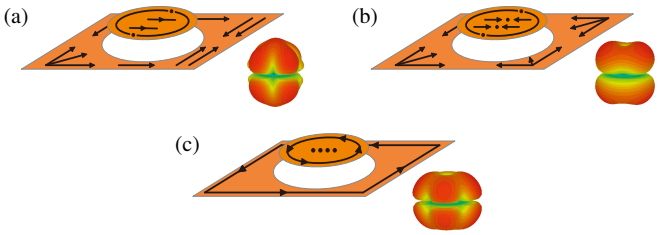

FIGURE 12. Characteristic current distributions and radiation patterns corresponding to the circular microstrip patch antenna with circular slot in ground plane, (a) mode J_1 at 32.06 GHz, (b) mode J_3 at 29.29 GHz, (c) mode J_4 at 19.70 GHz.

Figure 13 shows the current distributions and radiation patterns for the circular microstrip patch antenna with a circular slot in the patch at each resonance frequency. Modes J_1 and J_2 exhibit current flows predominantly in one direction, with J_1 characterized by vertical currents and J_2 by horizontal currents. This current distribution results in broadside radiation patterns with maximum radiation in the $+z$ direction. In contrast, mode J_3 shows two distinct variations in current direction, whereas mode J_4 demonstrates a combination of vertical and horizontal currents. These current arrangements produce radiation pat-

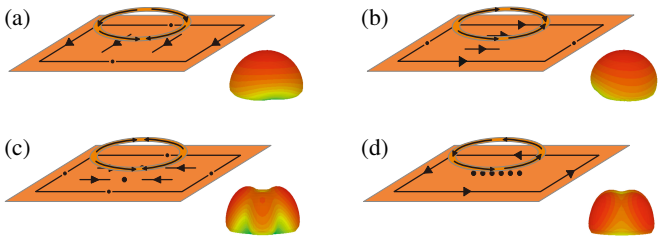

FIGURE 13. Characteristic current distributions and radiation patterns corresponding to the circular microstrip patch antenna with circular slot in patch, (a) mode J_1 at 19.95 GHz, (b) mode J_2 at 31.61 GHz, (c) mode J_3 at 20.43 GHz, (d) mode J_4 at 32.26 GHz.

terns perpendicular to the antenna's axis, with a null along the central alignment in the same direction. The measured directivities of the four resonant modes are 7.55 dBi, 7.38 dBi, 3.57 dBi, and 5.21 dBi, respectively.

The characteristic current distributions and radiation patterns corresponding to the microstrip ring resonator antenna with a circular slot in the ground plane at each of its resonance frequencies are shown in Fig. 14. Modes J_1 and J_4 exhibit two distinct variations in the current direction. This current configuration results in bi-directional radiation patterns with a null at the boresight, indicating suppressed radiation in the $\pm z$ directions. In contrast, modes J_2 and J_3 show horizontal current distributions, generating bidirectional radiation patterns with maximum field strengths in the $\pm z$ directions. The measured directivities of the four resonant modes are 4.39 dBi, 5.18 dBi, 4.6 dBi, and 4.09 dBi, respectively.

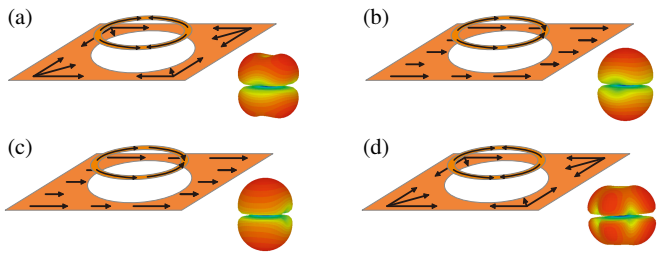

FIGURE 14. Characteristic current distributions and radiation patterns corresponding to the microstrip ring resonator antenna with circular slot in ground plane, (a) mode J_1 at 28.86 GHz, (b) mode J_2 at 21.11 GHz, (c) mode J_3 at 19.98 GHz, (d) mode J_4 at 19.75 GHz.

The characteristic current distribution and radiation patterns of the microstrip double-ring resonator antenna at each resonance frequency are shown in Fig. 15. It can be observed that the modes J_1 and J_3 have a high concentration of current flow within the rings, which indicates a stronger resonance effect at higher frequencies. The current distribution has a broadside radiation pattern with a maximum field strength in the $\pm z$ directions. The modes J_2 and J_4 have a slight change in the current distribution, which has a simpler distribution with a broader radiation pattern, indicating more efficient operation at lower frequencies compared with the operation of the modes J_1 and J_3. The measured directivities of the four resonant modes of the microstrip double-ring resonator antenna were 4.26 dBi, 3.16 dBi, 4.24 dBi, and 3.19 dBi, respectively.

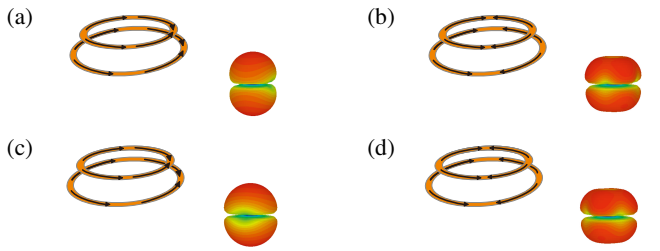

FIGURE 15. Characteristic current distributions and radiation patterns corresponding to the microstrip double-ring resonator antenna, (a) mode J_1 at 21.75 GHz, (b) mode J_2 at 29.06 GHz, (c) mode J_3 at 21.65 GHz, (d) mode J_4 at 29.10 GHz.

This study examined the influence of metamaterial slots on the performance of a circular microstrip patch antenna. The findings revealed that the presence of slots, either in the ground plane or patch, considerably affected the resonant modes, radiation patterns, and bandwidth of the antenna. The study also demonstrated that the radiation pattern depended on the position of the slots. The modes with currents concentrated around the slots exhibited broadside radiation patterns. The directivity results further showed that the use of metamaterial slots improved the efficiency and performance of antennas. The use of metamaterial slots improved the performance of antennas by optimizing the resonant frequency and bandwidth. Therefore, the use of metamaterial slots improved the performance of antennas and can be used in future wireless communication systems.

3.3. Analysis of Magnetic and Electric Metamaterial Structures for Enhanced Antenna Performance

Among various types of metamaterials, magnetic and electric metamaterial structures have gained considerable attention owing to their unique properties and potential applications in the development of complex antennas and electromagnetic devices.

In this study, we analyzed the performance characteristics of magnetic and electric metamaterial structures using numerical simulations based on characteristic modes. We also investigated the impact of various parameters on the performance of magnetic and electric metamaterial structures and improved the properties of metamaterial antennas. The first step was to analyze broadside-coupled split-ring resonators (BC-SRRs) and broadside-coupled complementary split-ring resonators (BC-CSRRs), which are well-known structures for designing metamaterials with magnetic and electric responses. These structures comprise sub-wavelength resonators that exhibit strong electromagnetic responses at specific frequencies. These structures find application in controlling wave propagation characteristics. The broadside-coupled SRR is composed of two face-to-face rings printed on both sides of the substrate material, Rogers RT5880. The two rings are parallel to each other. The SRRs have a small gap of 0.1 mm and a width of 0.4 mm. The outer radius of the first ring is 2.4 mm, whereas the outer radius of the second ring is 3 mm. The complementary split-ring resonator was used to design the BC-CSRR. The structure is similar in dimensions to the SRR and is depicted in Fig. 16.

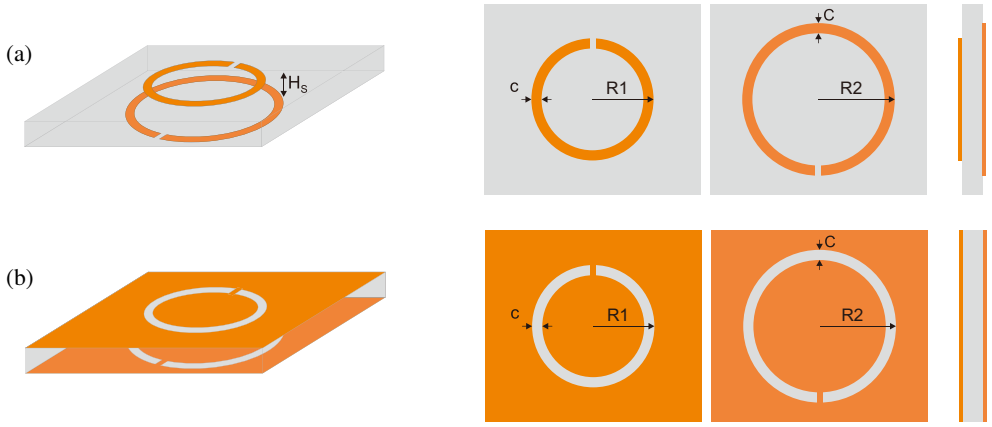

FIGURE 16. The geometry of (a) BC-SRR, (b) BC-CSRR.

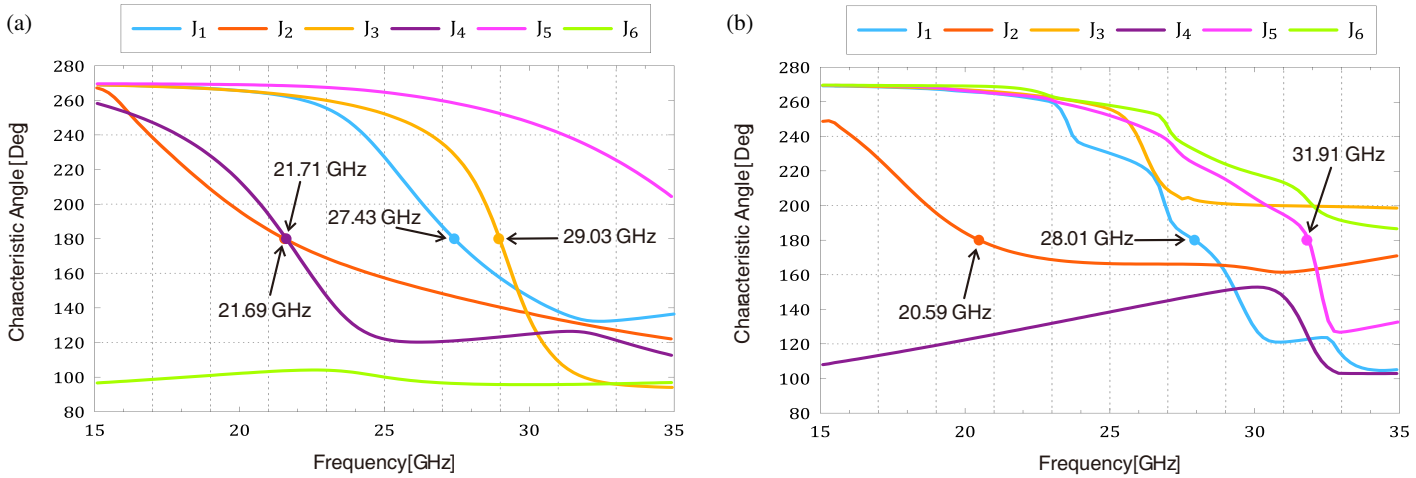

FIGURE 17. The variation with frequency of the characteristic angle for the first six modes of (a) BC-SRR, (b) BC-CSRR.

The variation of the characteristic angle with frequency for the first six modes of the BC-SRR and BC-CSRR antennas is shown in Fig. 17. As shown in Fig. 17(a), the BC-SRR antenna exhibits four degenerate electric resonant modes. Mode J_1 is an excellent radiator, resonating at 27.43 GHz with a bandwidth of 10.81%. Mode J_2 resonates at 21.69 GHz with a bandwidth of 49.04%. Modes J_3 and J_4 resonate at 14.75 GHz and 11.48 GHz, respectively, with bandwidths of 10.24% and 26.40%, respectively. The remaining modes, J_5 and J_6, store capacitive and inductive energy. In Fig. 17(b), the BC-CSRR antenna shows three degenerate magnetic resonant modes. Mode J_1 is an excellent radiator, resonating at 28.01 GHz with a bandwidth of 14.04%. Mode J_2 resonates at 20.59 GHz with an associated radiating bandwidth greater than 100%. Mode J_5 resonates at 31.91 GHz with a bandwidth of 14.60%. The other modes J_3 and J_6 store capacitive energy, whereas mode J_4 is a non-resonant mode with inductive energy.

Figure 18 shows the electromagnetic field distributions for the resonant modes of the BC-SRR for the upper and lower rings. As shown in Fig. 18(a), at modes J_1, J_2 and J_3, the E-field strength is higher. Mode J_4 is concentrated in the gap side of the ring. Fig. 18(b) shows that the E-field of modes J_1, J_3, and J_4 are condensed in almost the entire ring. The E-field of mode J_2 is concentrated on the right side of the upper ring. In Fig. 18(c), the H-field of mode J_1 has a high-intensity magnetic field compared to the modes J_2, J_3, and J_4, which have lower-intensity magnetic fields. Fig. 18(d) shows the H-field for the lower ring, and as noted, modes J_1 and J_2 have high-intensity magnetic fields compared to the modes J_3 and J_4 that have lower-intensity magnetic fields.

Figure 19 shows the electromagnetic field distributions for the resonant modes of the BC-CSRR for the upper and lower plates. As can be observed in Fig. 19(a), the E-field of the mode J_1 has a lower intensity electric field than the modes J_2, J_5, and J_4 that have high intensity. In Fig. 20(b), the electronic field of mode J_1 is located in the center of the plate, whereas mode $J5$ is centered along the edges of the antenna. In Fig. 19(c), all modes have lower-intensity magnetic fields. Fig. 19(d) depicts a lower-intensity H-field for modes J_1 and J_2, and a relatively medium density for mode J_5.

The analysis of the electromagnetic field distributions for the BC-SRR and BC-CSRR antennas reveals distinct characteristics for both the E-field and magnetic (H-field) fields across

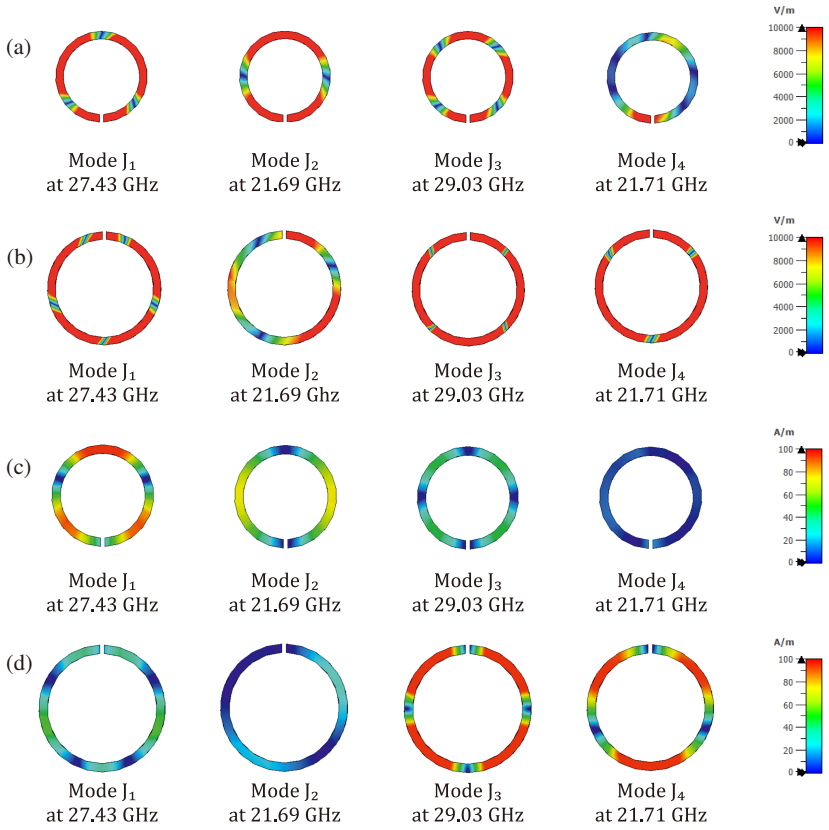

FIGURE 18. The field distributions of BC-SRR, (a) E-field for upper ring, (b) E-field for lower ring, (c) H-field for upper ring, (d) H-field for lower ring.

their resonant modes. In the BC-SRR antenna, the electric field at modes J_1, J_2, and J_3 is notably stronger, whereas mode J_4 is concentrated at the gap side of the ring. The electric field in the lower ring is more evenly distributed, with modes J_1, J_3, and J_4 exhibiting more uniform E-field intensity across nearly the entire ring, whereas mode J_2 shows a concentration of the E-field on the right side of the upper ring. The magnetic field intensity is the highest for mode J_1, with modes J_2, J_3, and J_4 displaying lower magnetic field intensities. For the BC-CSRR antenna, the electric field of mode J_1 is relatively weaker than modes J_2, J_5, and J_4, which show stronger electric fields.

The electric field for mode J_1 is concentrated at the center of the upper plate, whereas that for mode J_5 is concentrated along the edges of the antenna. From the perspective of the magnetic field, all modes have a low magnetic field intensity in the upper plate, whereas modes J_1 and J_2 have a low magnetic field strength, and mode J_5 has a medium magnetic field intensity in the lower plate. This analysis shows how the distributions of the electric and magnetic fields for the BC-SRR and BC-CSRR structures depend on the design of the antenna, with some modes affecting the overall response differently. This information is vital for the optimization of antennas for future communication systems.

Figure 20 presents the characteristic current distributions and corresponding radiation patterns for the resonant modes of the BC-SRR antenna, analyzed for both the upper and lower rings. For modes J_1 and J_4, the current distributions are symmetric and uniformly circulate across both rings, resulting in broadside radiation patterns that indicate efficient radiation along the primary axis. Finally, mode J_2 displays current flows predominantly concentrated near the gaps in the rings, leading to broader but less intense radiation. For mode J_3, the current alternates between segments of the rings, causing a slightly asymmetric radiation pattern. The measured directivities of the four resonant modes are 4.93 dBi, 4.25 dBi, 3.18 dBi, and 4.65 dBi, respectively. These results demonstrate the importance of resonant modes in controlling the electromagnetic response of the antenna, wherein J_1, J_2, and J_4 are found to have superior directivities, and J_3 provides information on local field effects.

Figure 21 presents the current distribution and radiation patterns of the BC-CSRR antenna's resonant modes for the upper and lower plates. For mode J_1 at 28.01 GHz, the current distribution is symmetrically distributed along the edges of the upper and lower plates. This gives a broadside radiation pattern with high directivity. For mode J_2 at 20.59 GHz, the current distribution has strong symmetry, which is concentrated towards the center of the upper and lower plates. This provides a broader radiation pattern with low directivity. For mode J_5 at 31.91 GHz, the current distribution is concentrated along the edges and corners of the upper and lower plates. This provides a highly directive radiation pattern with narrow lobes. The directivities of the four resonant modes were measured to be 6.54 dBi, 3.94 dBi, and 6.36 dBi, respectively. These results demonstrate the effects of resonant modes on the radiation characteristics of the BC-CSRR antenna, in which modes J_1 and J_5 have better di-

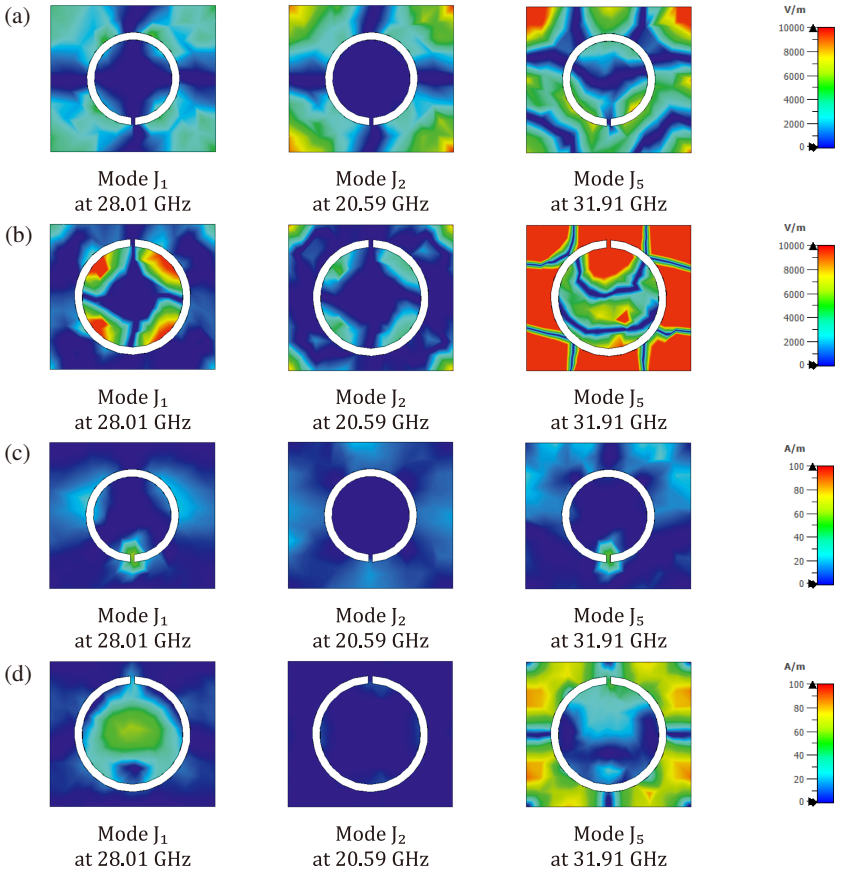

FIGURE 19. The field distributions of BC-CSRR, (a) E-field for upper plate, (b) E-field for lower plate, (c) H-field for upper plate, (d) H-field for lower plate.

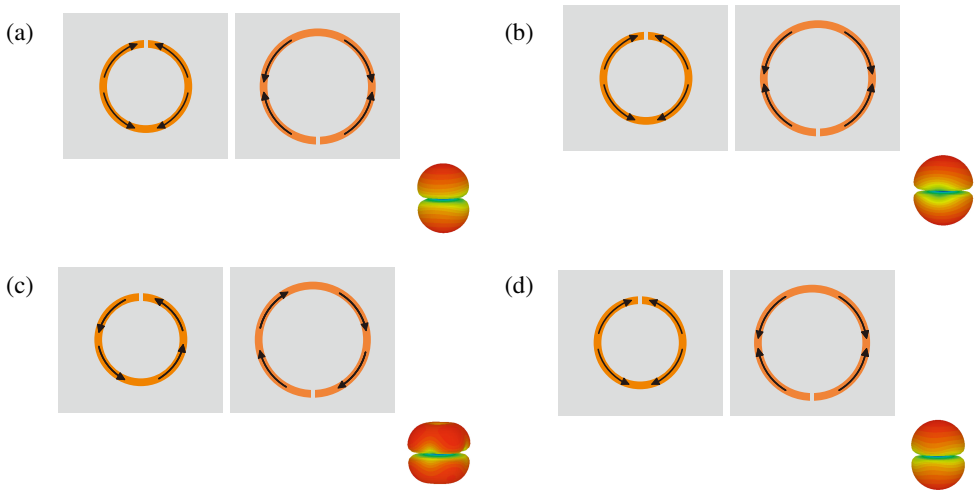

FIGURE 20. Current distributions and radiation patterns for the BC-SRR.

rectivities, and mode J_2 shows a balanced current flow and a broader radiation pattern.

The second set of structures under investigation includes EC-SRR and EC-CSRR structures, as shown in Fig. 22. These structures are considered exemplary for the realization of magnetic and electric metamaterials, which are characterized by the presence of an edge-coupled structure at the same level of the structure. It should be noted that the main aim of this study includes the analysis of the performance characteristics of metamaterial-based antennas through a detailed analysis of the unique properties of the EC-SRR and EC-CSRR structures. A detailed analysis of the EC-SRR and EC-CSRR structures was conducted to explore the electromagnetic properties of these structures, including the unique properties of the magnetic and electric components.

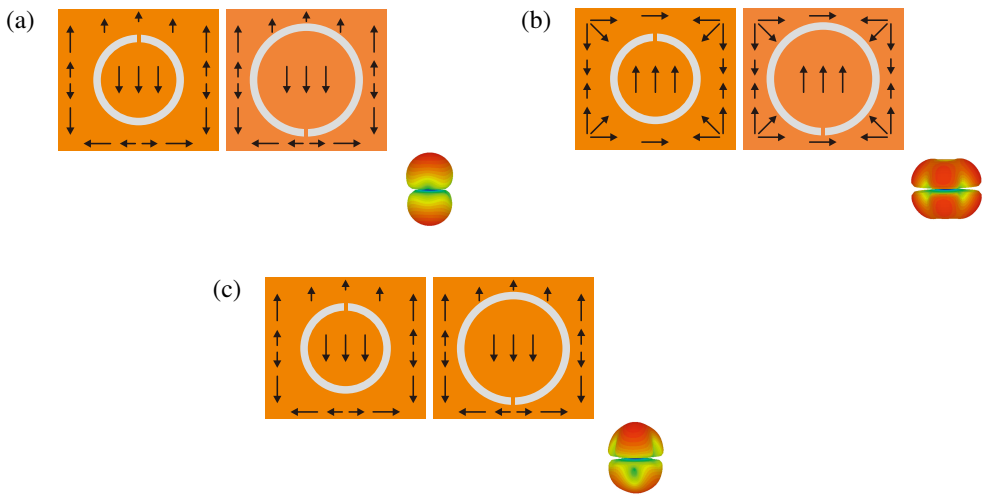

FIGURE 21. Current distributions and radiation patterns for the BC-CSRR.

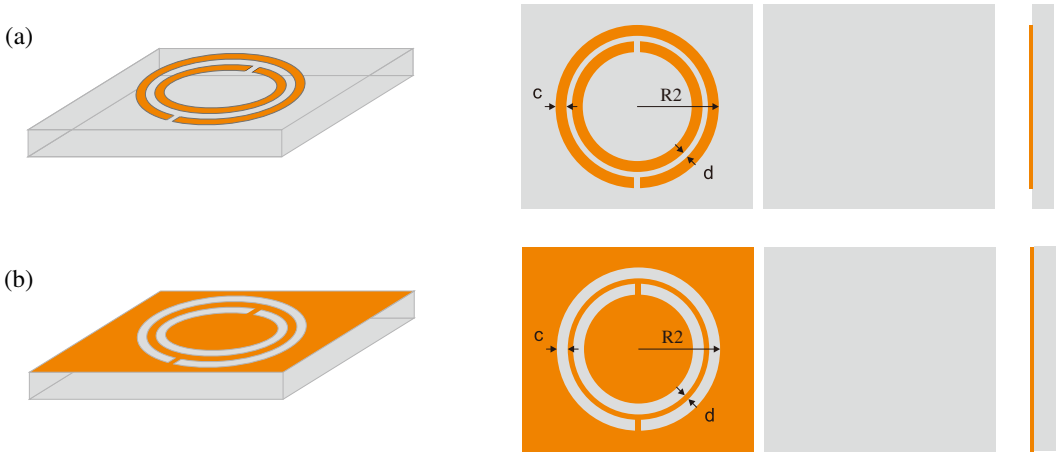

FIGURE 22. The geometry of (a) EC-SRR, (b) EC-CSRR.

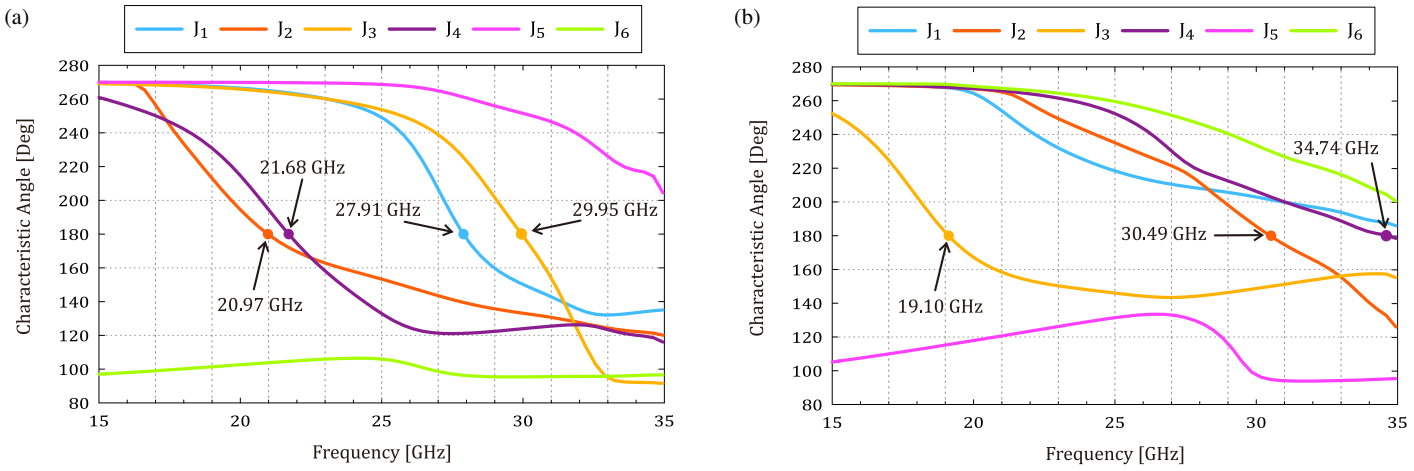

FIGURE 23. The CA for the first six modes of (a) EC-SRR, (b) EC-CSRR.

The characteristic angle variation with frequency for the first six modes of the EC-SRR and EC-CSRR antennas is presented in Fig. 23. As shown in Fig. 23(a), the EC-SRR has a degenerated electric resonant mode. Mode J_1 is a good radiator at resonance at 27.91 GHz with a bandwidth of 20.10%. Mode J_2 is in resonance at 20.97 GHz with a bandwidth of 51.15%. Mode J_3 is in resonance at 29.95 GHz with a bandwidth of 12.24%, and mode J_4 is in resonance at 21.68 GHz with a bandwidth of

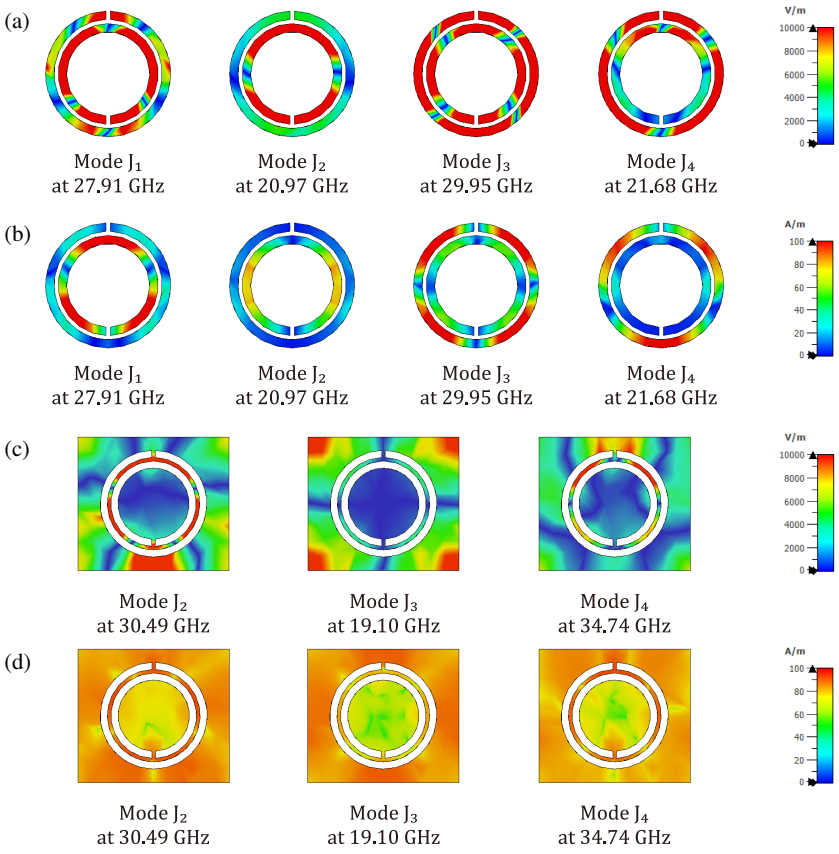

FIGURE 24. The field distributions of (a) E-field for EC-SRR, (b) H-field for EC-SRR, (c) E-field for EC-CSRR, (d) H-field for EC-CSRR.

27.82%. The other modes J_5 and J_6 store capacitive energy and inductive energy, respectively. As shown in Fig. 23(b), the EC-CSRR has a degenerated magnetic resonant mode. Mode J_2 is a good radiator at resonance at 30.49 GHz with a bandwidth of 26.10%. Mode J_3 is in resonance at 19.10 GHz, and mode J_4 is at 34.74 GHz with a radiating bandwidth greater than 100%. The other modes J_1 and J_6 store capacitive energy. The mode J_5 stores inductive energy.

Fig. 24 depicts the electromagnetic field distributions of EC-SRR and EC-CSRR antennas for different modes. The electric field distribution (a) for the EC-SRR antenna shows high localization of the electric field around the split edges of the resonator. The electric fields have different resonant frequencies for different modes, denoted by J_1, J_2, J_3, and J_4 at 27.91 GHz, 20.97 GHz, 29.95 GHz, and 21.68 GHz, respectively. The electric fields are localized around the edges of the resonator, which shows the accumulation of charge during the resonant frequency. The magnetic fields are localized around the resonator rings, as depicted in Fig. 24(b). The electric and magnetic fields are localized around the resonator ring, which shows the dipole characteristics of the antenna. The electric field distribution (c) for the EC-CSRR antenna is different because of the inverted geometry. The electric fields have different resonant frequencies for different modes, denoted by 30.49 GHz, 19.10 GHz, and 34.74 GHz. The complementary structure shows a different localization pattern for the fields compared to the EC-SRR. The fields are localized at positions that are complementary to the EC-SRR. The H-field distributions (d) for the EC-CSRR structures are more uniform and spread over the entire area of the complementary structures. These results indicate the resonance properties of the structures.

The results obtained for the characteristic current distribution and radiation patterns for the EC-SRR antenna in the four resonant modes are shown in Fig. 25. In mode J_1 at 27.91 GHz, the current distribution is symmetric, resulting in a high omnidirectional radiation pattern, which shows the potential of the antenna for focused signal transmission in broad-coverage applications. In mode J_2 at 20.97 GHz, the current distribution shows a shift, resulting in a directive radiation pattern for broad-coverage applications. In mode J_3 at 29.95 GHz, the current distribution shows concentration, resulting in high directivity with distinct lobes, which shows the suitability for precise radiation requirements. In mode $J4$ at 21.68 GHz, the current distribution shows moderate concentration, resulting in a broadside radiation pattern with the highest field strength along the $\pm z$ axes. The directivities for the four resonant modes obtained for the EC-SRR antenna were found to be 4.42 dBi, 4.15 dBi, 3.04 dBi, and 4.30 dBi, respectively. This results in the suitability of the EC-SRR antenna for tuning the operational requirements for different frequencies.

Figure 26 shows the current distribution and radiation patterns of the EC-CSRR antenna for the three resonant modes. For mode J_2 at 30.49 GHz, the current distribution is highly complex and is characteristic of a higher-order resonance mode.

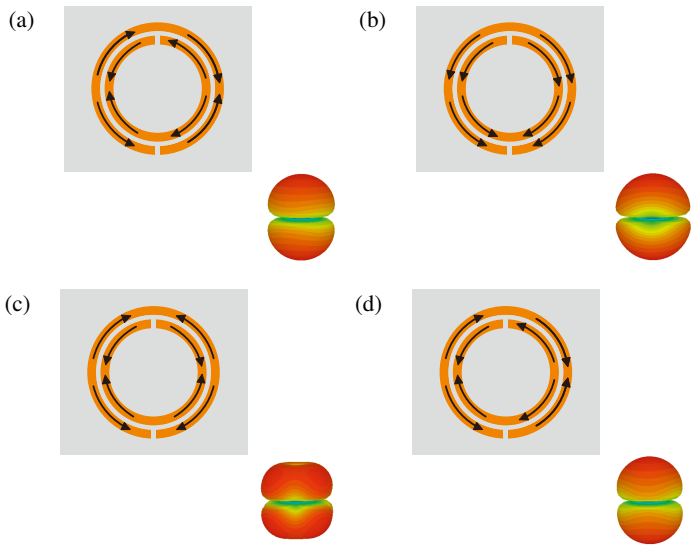

FIGURE 25. Current distributions and radiation patterns for the EC-SRR.

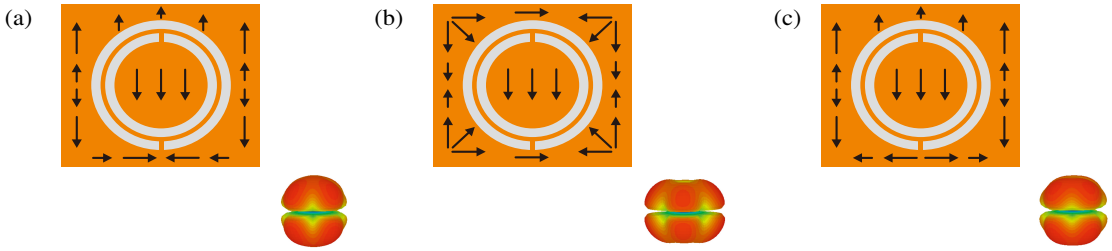

FIGURE 26. Current distributions and radiation patterns for the EC-CSRR.

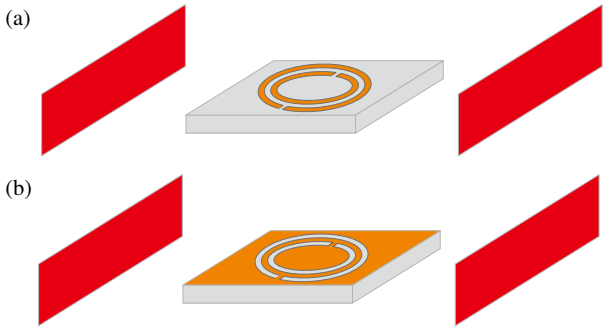

FIGURE 27. The antennas excited by the waveguide, (a) EC-SRR, (b) EC-CSRR.

Hence, it is a higher-order mode. The radiation pattern is highly directive for this mode and is suitable for applications, where focused transmission of the signal is required. In contrast, for mode J_4 at 34.74 GHz, there is a symmetric current flow along the inner and outer edges of the resonator structure. The radiation pattern is less directive than that of J_2 and has a wider beam coverage, which is advantageous for wider signal dissemination. The measured directivities for the four resonant modes were 3.97 dBi, 3.13 dBi, and 4.16 dBi, respectively. The EC-CSRR antenna has demonstrated versatility with respect to its performance over a range of frequencies, making it suitable for a range of needs.

This study demonstrates the considerable potential for improving the performance of magnetic and electrical metamaterial structures, such as BC-SRR, BC-CSRR, EC-SRR, and EC-CSRR antennas. In particular, the analysis of the electromagnetic properties has revealed the impact that the resonant modes can have on the radiation properties, directivity, and fields. The results indicate that the BC-SRR structures possess high electric fields and symmetric currents, resulting in efficient broadside radiation patterns with moderate directivity. Similarly, BC-CSRR antennas have shown improvement in directivity for modes in which current concentrations have aligned with the structural edges, confirming their applicability for high-frequency use. The edge-coupled designs EC-SRR and EC-CSRR have demonstrated the effect of the geometrical arrangement on the interaction between the magnetic and electric resonances, which will enable further optimization of the radiation performance. From this detailed analysis, it is clear that this analysis offers valuable information regarding the design aspects of antennas based on metamaterials. The proposed antenna is suitable for modern microwave and millimeter-wave applications, such as 5G communication systems, automotive radar, satellite communications, and microwave imaging systems. For such applications, antennas capable of operating at wideband frequencies have stable radiation properties, and are small in size are needed. The new antenna meets all the aforementioned criteria because of its wideband capabilities, which

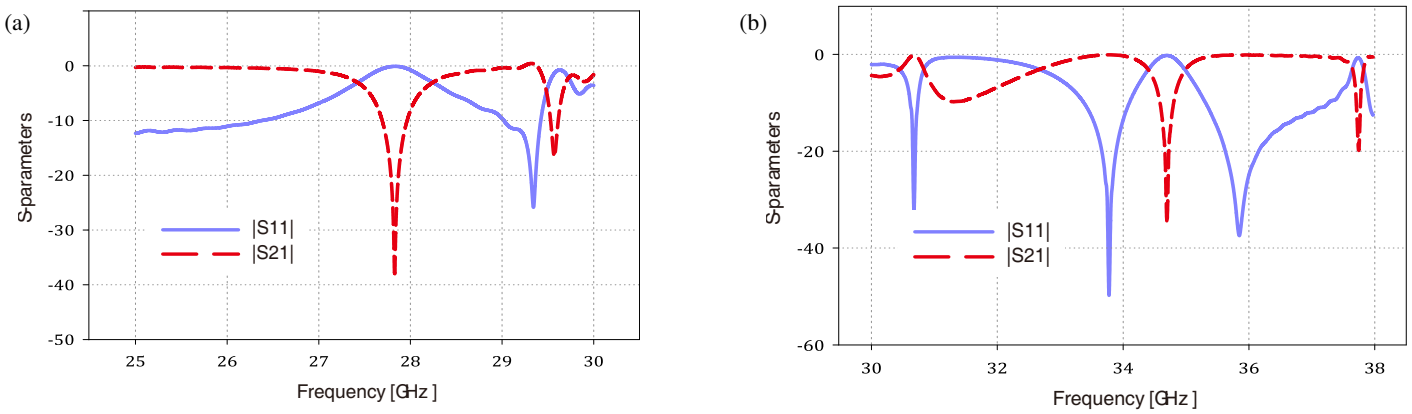

FIGURE 28. Simulated plots of S-parameters, (a) EC-SRR, (b) EC-CSRR.

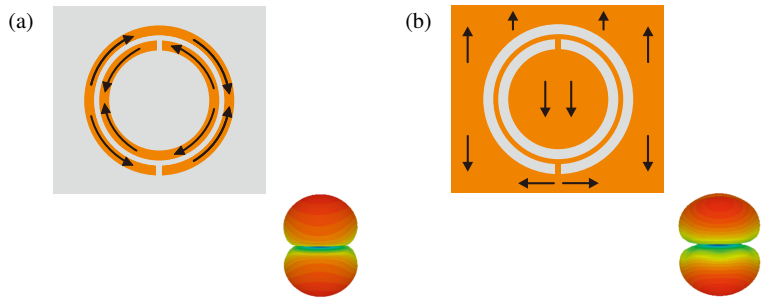

FIGURE 29. Current distributions and radiation patterns for (a) EC-SRR, (b) EC-CSRR.

result from the superposition of several characteristic modes and the ability to provide consistent radiation patterns with high directivity. Besides, the presence of metamaterial structures allows for the improved manipulation of electromagnetic parameters.

4. EXCITATION OF RESONANCE IN METAMATERIAL ANTENNAS WITH WAVEGUIDE

For the purpose of precision and accuracy of results obtained with characteristic modes, the specific resonance mode of the split-ring resonator and complementary split-ring resonator is intentionally excited using a waveguide, as depicted in Fig. 27.

This intentional excitation is performed to excite the high-directivity mode of the antennas. For the SRR structure, the resonance frequency is set to 27.91 GHz, and for the CSRR structure, the resonance frequency is set to 34.74 GHz. The response of the antenna is validated by performing a thorough analysis of the S-parameters of the antenna to determine its reflection and transmission characteristics. The metamaterial antennas are placed strategically between two waveguide ports, along the negative and positive x-axes, and oriented perpendicular to the z-axis, as illustrated in the figure. The placement of the metamaterial antennas between the waveguide ports is intended to control the excitation response of the designed antennas. This arrangement enables the exploration of the antenna resonance modes, with particular attention to the high-directivity mode, which is of particular importance in the design of the antenna for specific purposes. The method of excitation ensures efficient energy coupling to the antenna, thus enabling the precise tuning of the resonant frequency of the antenna. The results obtained from the analysis of the S-parameters are of particular importance in understanding the performance of the antenna, thus verifying the high-directivity mode of each structure.

Figure 28 presents the simulated S-parameters for the EC-SRR and EC-CSRR antennas. As shown in Fig. 28(a), the EC-SRR is in resonance at 27.9 GHz, with an S_{21} magnitude of -38.53 dB. The -10 dB bandwidth of S_{21} extends from 27.692 GHz to 27.965 GHz. In Fig. 28(b), the EC-CSRR reaches resonance at 34.7 GHz, with an S_{21} magnitude of -34.8 dB, and the -10 dB bandwidth of S_{21} ranges from 34.589 GHz to 34.804 GHz. Notably, the results reveal a remarkable agreement between the outcomes derived from the characteristic modes and the performance of the S-parameters, although there is some variation in the bandwidth. This difference can be accounted for by the approximations made during the calculation of the electrical design parameters.

Figure 29 shows the distribution of currents and radiation patterns of the antenna designs for both EC-SRR and EC-CSRR designs when excited. It can be seen that the currents on the surfaces are predominantly found in the resonating elements, thus indicating an effective excitation of the dominant modes. From the plots of their radiation patterns, it can be noted that the modes play a critical role in the formation of the radiated field. The measured directivities of the resonant modes are 4.98 dBi and 6.22 dBi, respectively. These results verify the accuracy and consistency of the characteristic modes in predicting the response of the structure to the electromagnetic field. The re-

sults obtained are consistent, and their comparison proves the efficiency of the characteristic modes, in addition to their importance in predicting the response of the structure, which is necessary for improving the efficiency of metamaterial antenna structures.

5. CONCLUSION

In this study, we have conducted a detailed analysis and experimental validation, which underscores the critical role of characteristic mode analysis in optimizing the performance of metamaterial antennas for future wireless communication systems. The detailed analysis of the fundamental antenna structures to understand the behavior of each individual element within the structure, and by integrating various slot configurations into microstrip antennas, has demonstrated that structural modifications play an important role in influencing the resonant frequencies and radiation patterns. We have demonstrated that the electromagnetic resonant modes of microstrip patch antennas and metamaterial structures can have a great impact on improving the efficiency of antennas. The simulation results indicate that the values of the CMA and S-parameter are very close, proving that the proposed designs are robust. The strategic use of waveguide excitation is another factor that proves resonance behavior, ensuring that these antennas will work in real-life applications. This study presents an understanding of the potential of metamaterial-based antennas to revolutionize the way we address the challenges of next-generation wireless networks.

REFERENCES

[1] Pozar, D. M., "Microstrip antennas," *Proceedings of the IEEE*, Vol. 80, No. 1, 79–91, Jan. 1992.

[2] Garg, R., P. Bhartia, I. Bahl, and A. Ittipiboon, *Microstrip Antenna Design Handbook*, Artech House, 2001.

[3] Wheeler, H., "Small antennas," *IEEE Transactions on Antennas and Propagation*, Vol. 23, No. 4, 462–469, Jul. 1975.

[4] Venugopal, V., A. P. Abhilash, R. K. Raj, and T. Mathew, "CPW-fed minkowski island fractal slot antenna for wideband application," *Progress In Electromagnetics Research Letters*, Vol. 125, 9–15, 2025.

[5] Zhang, Z., S. Cao, and J. Wang, "Azimuth-pattern reconfigurable planar antenna design using characteristic mode analysis," *IEEE Access*, Vol. 9, 60 043–60 051, 2021.

[6] Robinson, J. and Y. Rahmat-Samii, "Particle swarm optimization in electromagnetics," *IEEE Transactions on Antennas and Propagation*, Vol. 52, No. 2, 397–407, Feb. 2004.

[7] Garbacz, R. J. and R. H. Turpin, "A generalized expansion for radiated and scattered fields," *IEEE Transactions on Antennas and Propagation*, Vol. 19, No. 3, 348–358, 1971.

[8] Harrington, R. and J. Mautz, "Theory of characteristic modes for conducting bodies," *IEEE Transactions on Antennas and Propagation*, Vol. 19, No. 5, 622–628, Sep. 1971.

[9] Harrington, R. and J. Mautz, "Computation of characteristic modes for conducting bodies," *IEEE Transactions on Antennas and Propagation*, Vol. 19, No. 5, 629–639, Sep. 1971.

[10] Pendry, J. B., A. J. Holden, D. J. Robbins, and W. J. Stewart, "Magnetism from conductors and enhanced nonlinear phenomena," *IEEE Transactions on Microwave Theory and Techniques*, Vol. 47, No. 11, 2075–2084, Nov. 1999.

[11] Shelby, R. A., D. R. Smith, and S. Schultz, "Experimental verification of a negative index of refraction," *Science*, Vol. 292, No. 5514, 77–79, Apr. 2001.

[12] Linden, S., C. Enkrich, M. Wegener, J. Zhou, T. Koschny, and C. M. Soukoulis, "Magnetic response of metamaterials at 100 terahertz," *Science*, Vol. 306, No. 5700, 1351–1353, Nov. 2004.

[13] Capolino, F., *Theory and Phenomena of Metamaterials*, CRC Press, 2009.

[14] Soukoulis, C. M., S. Linden, and M. Wegener, "Negative refractive index at optical wavelengths," *Science*, Vol. 315, No. 5808, 47–49, Jan. 2007.

[15] Shalaev, V. M., "Optical negative-index metamaterials," *Nature Photonics*, Vol. 1, No. 1, 41–48, Jan. 2007.

[16] Schurig, D., J. J. Mock, B. J. Justice, S. A. Cummer, J. B. Pendry, A. F. Starr, and D. R. Smith, "Metamaterial electromagnetic cloak at microwave frequencies," *Science*, Vol. 314, No. 5801, 977–980, Nov. 2006.

[17] Baena, J. D., J. Bonache, F. Martin, R. M. Sillero, F. Falcone, T. Lopetegi, M. A. G. Laso, J. Garcia-Garcia, I. Gil, M. F. Portillo, and M. Sorolla, "Equivalent-circuit models for split-ring resonators and complementary split-ring resonators coupled to planar transmission lines," *IEEE Transactions on Microwave Theory and Techniques*, Vol. 53, No. 4, 1451–1461, Apr. 2005.

[18] Solymar, L. and E. Shamonina, *Waves in Metamaterials*, Oxford University Press, 2009.

[19] Liu, Z., H. Lee, Y. Xiong, C. Sun, and X. Zhang, "Far-field optical hyperlens magnifying sub-diffraction-limited objects," *Science*, Vol. 315, No. 5819, 1686, Mar. 2007.

[20] Cummer, S. A., J. Christensen, and A. Alù, "Controlling sound with acoustic metamaterials," *Nature Reviews Materials*, Vol. 1, No. 3, 1–13, 2016.

[21] Holloway, C. L., E. F. Kuester, J. Baker-Jarvis, and P. Kabos, "A double negative (DNG) composite medium composed of magnetodielectric spherical particles embedded in a matrix," *IEEE Transactions on Antennas and Propagation*, Vol. 51, No. 10, 2596–2603, Oct. 2003.

[22] Boardman, A. D., P. Egan, L. Velasco, and N. King, "Control of planar nonlinear guided waves and spatial solitons with a left-handed medium," *Journal of Optics A: Pure and Applied Optics*, Vol. 7, No. 2, S57, Feb. 2005.

[23] Liu, R., T. J. Cui, D. Huang, B. Zhao, and D. R. Smith, "Description and explanation of electromagnetic behaviors in artificial metamaterials based on effective medium theory," *Physical Review E*, Vol. 76, No. 2, 026606, Aug. 2007.

[24] Belov, P. A., R. Marqués, S. I. Maslovski, I. S. Nefedov, M. Silveirinha, C. R. Simovski, and S. A. Tretyakov, "Strong spatial dispersion in wire media in the very large wavelength limit," *Physical Review B*, Vol. 67, No. 11, 113103, Mar. 2003.